

Preliminary Finite-Source Study of the February 21, 2008 Wells, Nevada Earthquake

by

Douglas S. Dreger, Sean R. Ford, and Isabelle Ryder
Berkeley Seismological Laboratory

2011

ABSTRACT

Seismic moment tensor and finite-source analyses are performed for the 21 February 2008 Wells, Nevada earthquake. Using complete, intermediate period (10-50s), regional waveforms, and assuming the U. S. Geological Survey (USGS)-reported hypocenter, the best-fit moment tensor solution is a normal mechanism that strikes approximately northeast-southwest, consistent with the trend of Basin and Range faulting in the area. A moment magnitude (M_W) of 5.9 was obtained. Using three-component displacement waveforms (period < 50s) from nearby EarthScope Transportable Array (TA) stations and the source parameters from the moment tensor analysis, a finite-source solution is calculated. The best-fit rupture plane dips southeast and the rupture velocity is 2.8 km/s (0.78β), though the rupture velocity is not well constrained. The preferred solution allowing for variable rake and rise-time results in a compact slip distribution where the maximum slip is 1-3 km deeper than the hypocenter and is skewed to the southeast, yielding a seismic moment of $1.25e25$ dyne cm (M_W 6.0). Finally, a finite-source inversion using interferometric synthetic aperture radar (InSAR) line-of-sight displacements results in a similar slip pattern, though the depth is decreased by about 5 km, and yields a scalar seismic moment of $1.68e25$ dyne cm (M_W 6.1).

INTRODUCTION

On 21 February 2008 the Wells, Nevada earthquake struck approximately 10 km northeast of town (figure 1b), and inflicted substantial damage to the historic district with partial collapse of unreinforced masonry buildings (dePolo, 2008). The earthquake occurred in northeastern Nevada where seismicity rates are low, and seismic network coverage is sparse. However, at the time of the earthquake the EarthScope Transportable Array (TA) was deployed providing unprecedented coverage of the intermountain west. Unfortunately there were no strong motion observations near the damaged area.

In the days following the earthquake seismic moment tensor and finite-source inversions using the EarthScope TA data were performed to determine the faulting mechanism, the causative rupture plane, and to investigate source rupture effects on the levels of strong shaking in the town of Wells, Nevada. Here we document that work as well as present an updated finite-source model, and analyze the surface deformation obtained from InSAR.

DATA AND METHODS

Moment Tensor Inversion

Three component waveform data from TA and US stations less than 300 km away from the event (figure 1) were obtained from the IRIS data center. The data was instrument corrected, integrated to displacement, and band-pass filtered using a 6th order acausal Butterworth filter with corners at 0.02 and 0.05 Hz. Green's functions were computed using the Song and others (1996) velocity model (table 1) for source depths of 7 and 10 km to test the initially reported depths for the event. Details of the inversion method can be found in Minson and Dreger (2007), and as applied in the western US in Ford and others (2009).

Table 1. Velocity model (Song and others, 1996).

Thick (km)	V_α (km/s)	V_β (km/s)	ρ (g/cc)	Q_α	Q_β
2.5	3.6	2.05	2.2	100.0	40.0
32.5	6.1	3.57	2.8	286.0	172.0
∞	7.85	4.53	3.3	600.0	300.0

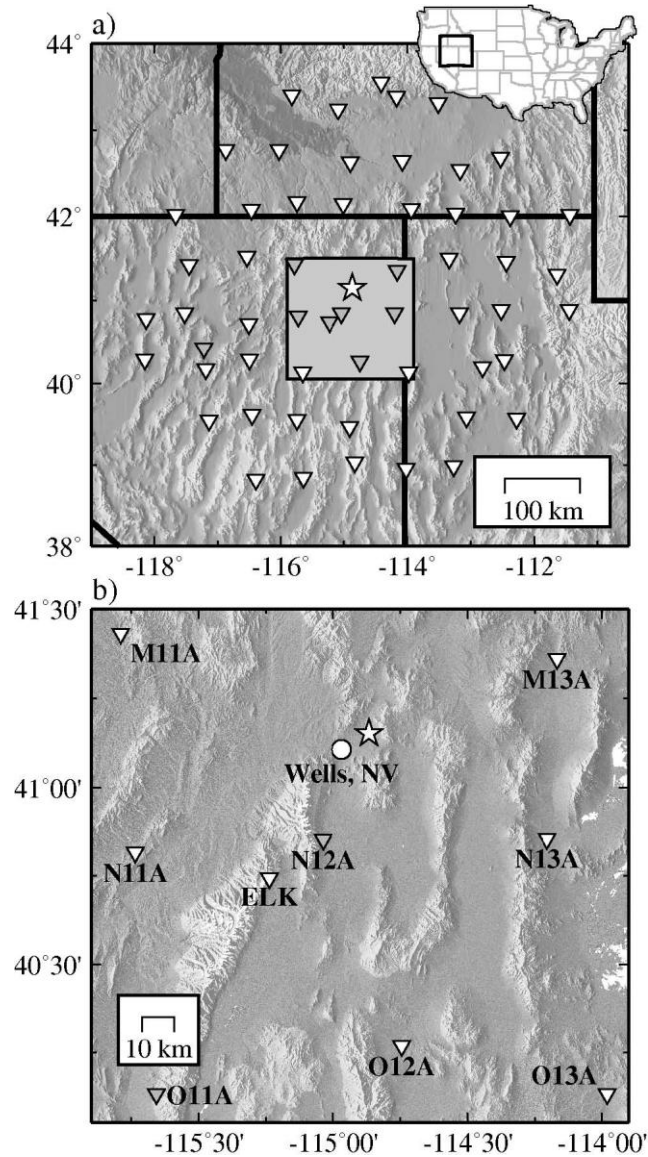


Figure 1. a) Regional map of stations (triangles) within 300 km of the event (star) and those used in the moment tensor inversion (white triangles). The map area is outlined in the inset US map and the area shown in b) is outlined with a gray square. b) Local map of stations used in the finite source inversion (white triangles). The town of Wells, Nevada is marked by a circle.

The Green's functions for the moment tensor inversion were aligned with the data based on the USGS location and origin time, but this alignment was allowed a shift of -4 to 4 sec to allow for an optimal match between the data and

Green's functions to reduce the effects of uncertainties in the velocity structure, the hypocenter, and the origin time. It is noted that paths to the north tended to require positive shifts (maximum of 3 seconds) indicating a too-slow velocity model, whereas to the south the shifts were negative (maximum of -3 seconds) indicating the velocity model was too fast. Considering all of the stations, the average time shift was 0.3 seconds, indicating that on average the Song and others (1996) velocity model is a reasonable approximation to crustal structure.

Finite-Source Inversion

For the finite-source inversion we examined three-component, broadband displacement waveforms from the 8 closest TA and US stations (figure 1b). We focused on these closest stations because they provide very good azimuthal coverage of the source, and they should have smaller cumulative timing errors due to errors in the assumed velocity model than more distant stations. During the initial examination of the waveform data it was found that station N12A exhibited a non-linear instrument response and was therefore removed from further analysis.

The data were processed similarly to the moment tensor analysis except that only a high-pass filter with a corner at 0.02 Hz was used. As shown in the following, the displacement waveforms are rich in long-periods due to the source, and therefore a low-pass filter was not applied. Green's functions were computed using the same velocity model as in the moment tensor analysis. Details of the inversion method can be found in Dreger and Kaverina (2000) and Kaverina and others (2002).

Geodetic Observations and Inversion

The coseismic deformation from ALOS PALSAR (operated by the Japanese Space Agency) InSAR data was obtained from a pair of ascending scenes (track angle N13.5W; look angle 34.3 degrees), the pre-event scene on 19 Dec 07 64 days before the event and the post-event scene on 20 Mar 08, 28 days following the event. These data were processed resulting in estimates of the change in distance between the ground surface and the imaging satellite, the line-of-sight change (Δ LOS). Δ LOS from the preferred seismic slip model is computed for comparison with observations assuming a Poisson half-space elastic structure using the algorithms of Okada (1985), and the method illustrated in Kaverina and others (2002). The Δ LOS data are then inverted for the slip distribution using the same methods.

RESULTS

Seismic Moment Tensor Inversion

The data and synthetics for 47 stations between 100 and 300 km used in the moment tensor inversion are compared in figure 2. The best-fit deviatoric moment tensor source model that produced the synthetic waveforms shown in figure 2 (gray traces) is given in figure 3 along with a polar plot representing the azimuth and distance for each station that went into the inversion. The stations provide exceptional azimuthal coverage. The fit is very good (83.6% variance reduction, with 100% being perfect fit). The scalar seismic moment ranges from $7.828.89 \times 10^{24}$ dyne-cm (M_w 5.9-6.0) for source depths of 7 and 10 km, respectively. The solution for a source depth of 7 km is preferred since it results in slightly better fit. This depth is also consistent with the USGS body wave CMT depth. The best-fit source parameters obtained from the moment tensor analysis are listed in table 2 and compared with other published results. The solutions are very comparable.

Table 2. Reported Wells earthquake mechanisms

Strike	Rake	Dip	Moment (M_w) (10^{24} dyne-cm)	Depth (km)	Source
205°/35°	-96°/-82°	50°/40°	7.8 (5.9)	7	This study
230°/9°	-55°/-114°	40°/58°	13 (6.0)	10	USGS CMT
206°/19°	-86°/-96°	58°/33°	6.8 (5.8)	7	USGS Body-wave MT
205°/25°	-90°/-90°	50°/40°	8.3 (5.9)	11	SLU MT
203°/36°	-99°/-81°	47°/44°	13 (6.0)	14.1	Global CMT

Finite-Source Inversion

In the days following the event there was uncertainty as to whether the causative fault was east dipping or west dipping. Automatic locations of aftershocks were not able to discern the fault plane. Using the approach described in Dreger and Kaverina (2000), both possible fault planes from the moment tensor analysis were tested assuming a simple planar fault model with the orientation found from the moment tensor inversion, and assuming both constant rise time and slip direction, again from the moment tensor results. In order to account for some of the error in timing between observations and Green's functions due to the use of a simplified velocity structure to compute Green's functions as well as uncertainty in the origin time and hypocenter location of the earthquake, we performed a systematic search for an optimum time shift as was done in the moment tensor inversion. Here we only allowed the stations to be shifted by the same amount, and the best time shift, defined as the one yielding the best fit using the variance reduction metric, advanced the data by 2 seconds (testing a range of -4 to 4 seconds) with respect to the Green's functions. This time shift aligned the first arriving P-waves for the most part, however more complete examination of time shifts between observations and Green's functions, allowing for different values at each station, is needed and will be the focus of future work.

The results show that the southeast-dipping plane was the rupture plane (figure 4). A best-fitting rupture velocity of 2.8 km/s (0.78β), was found for this rupture plane. Figure 4 shows that while the causative plane is well determined with more than a 10% difference in variance reduction between the two planes, the rupture velocity is not well constrained by the broad peak in the variance reduction plot. The best-fitting variance reduction was 54%, and as figure 5a shows the observed broadband data (figure 5) is well matched. It is interesting to note that station ELK is nearly nodal for all three components indicating that the takeoff angle for the surface wave energy is near the null-axis of the double-couple focal mechanism. This suggests that the rupture had a relatively simple planar fault with little variation in slip direction. In other words the rupture had an effectively constant radiation pattern at least at the azimuth to ELK.

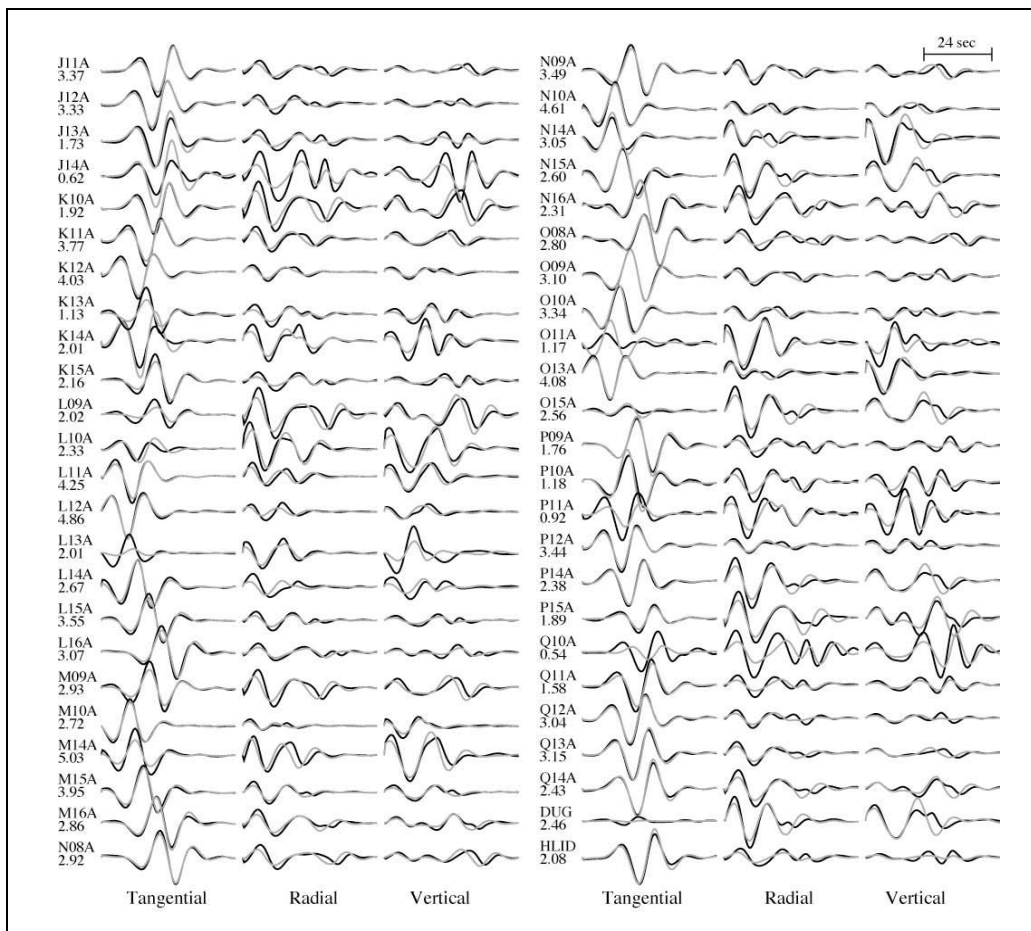


Figure 2. Displacement data (black) compared with synthetic waveforms (gray) produced by the mechanism shown in figure 3 at a depth of 7 km. The data and synthetics are filtered with a 6 pole acausal Butterworth bandpass between 0.02 to 0.05 Hz. The station name and maximum displacement in 10⁻² cm are to the left of each three-component waveform.

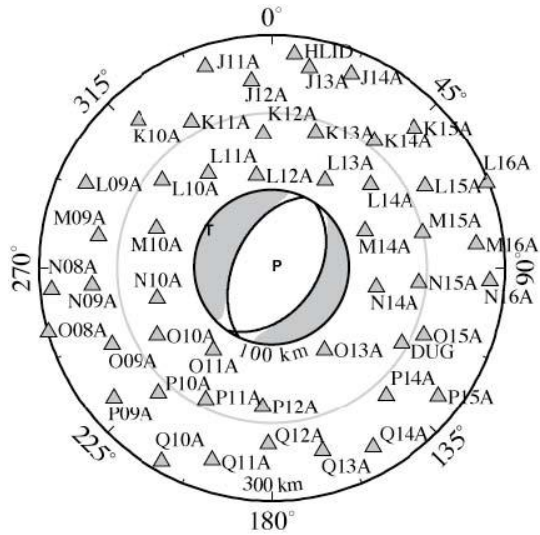


Figure 3. Best-fit deviatoric moment tensor solution at center of polar plot of station locations relative to the event. Compressional quadrants are shaded and the T and P axes are noted. The radius of the focal mechanism represents a distance of 100 km, the gray circle 200 km, and the outer circle of the polar plot 300 km.

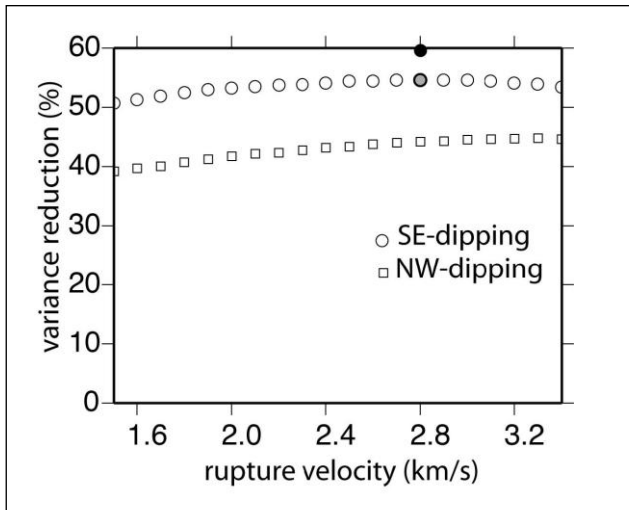


Figure 4. Waveform fit (parameterized by variance reduction) as a function of fault plane and rupture velocity for the constant rake and constant rise time model. The best-fit (54%, gray circle) occurs at a rupture velocity of 2.8 km/s on the southeast-dipping plane. The variable rake and rise time model shown in figure 6b fits the data slightly better (60%, black circle).

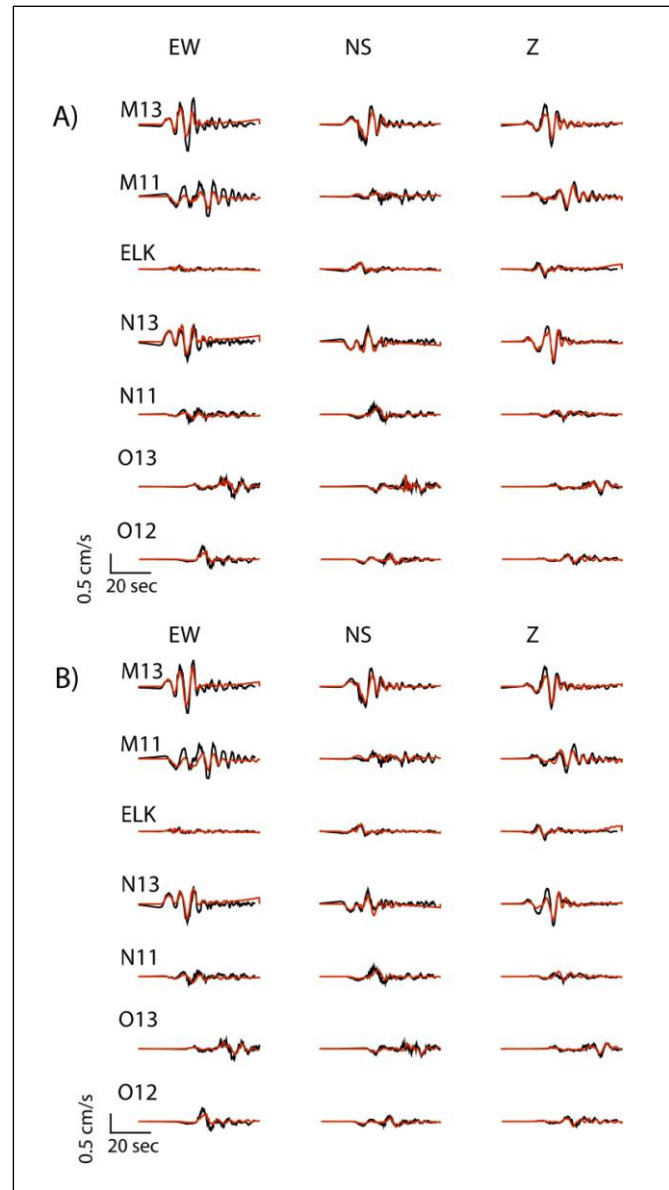


Figure 5. Displacement data (black) compared with synthetic waveforms (gray) produced by the finite-source models shown in figure 6, a) for the initial model, and b) the preferred variable rake, and multiple time window inversion model. The data and synthetics are filtered with a 6pole acausal Butterworth high-pass at 0.02 Hz.

Smith and others (2008) relocated the mainshock and aftershocks, and found that the aftershocks define a plane striking N40°E with a 55° dip to the SE, consistent with the finite-source results. The hypocenter coordinates for the mainshock reported by Smith and others (2008) are 41.167 N latitude, 114.877W longitude and 6.98 km depth with an origin time of 14:16:02.67 PST. The orientation of the fault plane interpreted from the relocated aftershocks is within the uncertainties of the long-period moment tensor analyses represented by the multiple solutions (table 2). We updated the finite-source inversion results by considering the revised hypocenter coordinates and aftershock-inferred fault orientation. In addition we allowed the source model to account for spatial variations in slip direction (rake) and slip rise time using the Hartzell and

Heaton (1983) multiple time window parameterization (e.g. Kaverina and others, 2002). We used the same data time shifts as described above, and assumed the best fitting rupture velocity of 2.8 km/s. As seen in figure 6b the slip in this model collapses toward the hypocenter. The primary asperity in this model extends to the southeast and down dip of the hypocenter. The main slip in this model is located in a region with relatively fewer aftershocks with a peak slip of 103 cm in the southeast asperity. Fifty cm of this slip occurs in the first 0.3 second time window indicating a 150 cm/s peak slip velocity. The remainder of slip accumulated more slowly over the remaining 1.3 second maximum rise time. The scalar seismic moment was determined to be 1.25×10^{25} dyne cm corresponding to a moment magnitude of 6.0. This model improves the fit to the data slightly increasing from the variance reduction from 54% to 60% (figure 4), and as the waveform comparison in figure 5b shows the matches are quite good. Furthermore, the nodal nature of ELK is preserved by this model. Future work of course must examine the rupture velocity parameter space as well as investigate the sensitivity of the results to perturbations in fault orientation and hypocenter allowed by the uncertainties in those estimates.

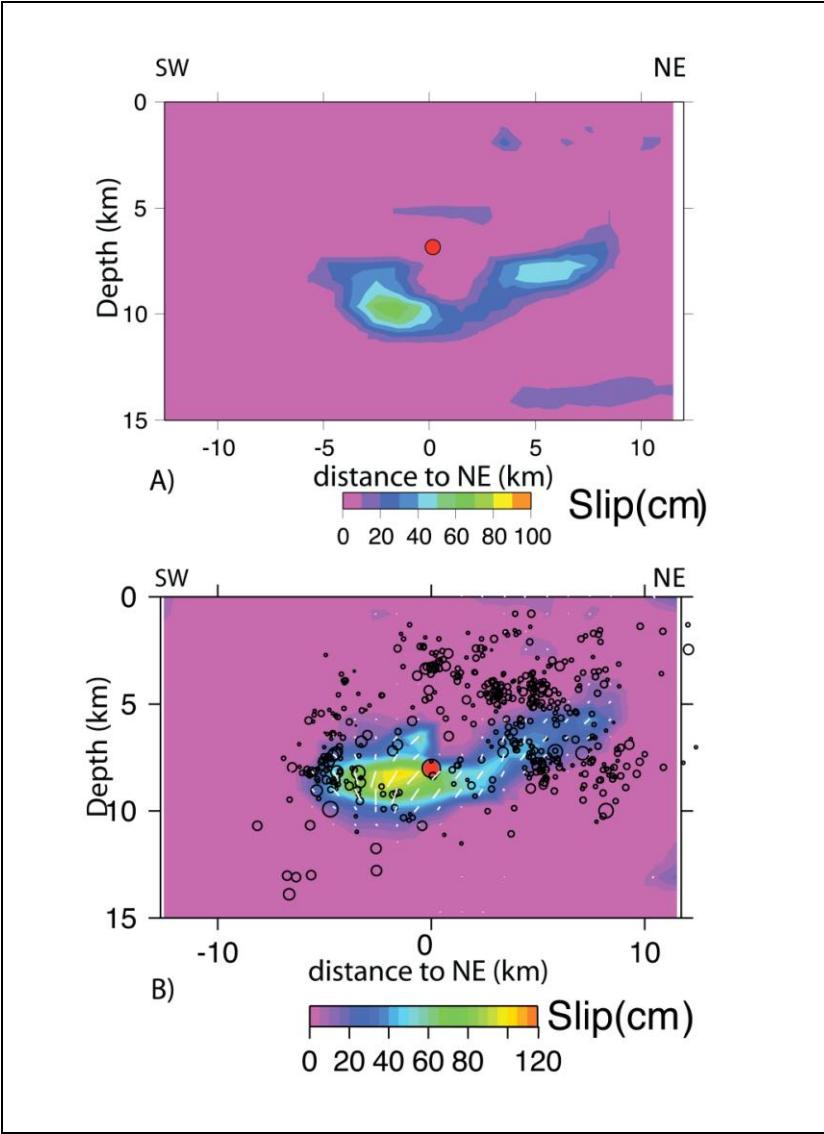


Figure 6. A) Finite-fault solutions assuming a rupture velocity of 2.8 km/s, constant rise time and slip direction for the southeast-dipping plane from the moment tensor inversion. Hypocenter is the red circle. B) Slip model allowing for variable rake and rise-time and using the Smith and others (2008) fault orientation (strike = N40E, dip = 55° to the southeast) obtained from the aftershock distribution. The rupture velocity is 2.8 km/s. The aftershock hypocenters within 1 km of the fault-plane are plotted with black circles where the diameter is a function of magnitude. The hypocenter is shown as the red circle and the slip vectors are shown as white bars. Note that the slip is located in an area of fewer aftershocks.

Analysis of Geodetic (SAR) Data

In figure 7a the unwrapped line-of-sight deformation (ΔLOS), calculated from a pre-event scene on December 19, 2007 and a post-event scene on March 20, 2008, shows an elliptical distribution with a maximum ΔLOS increase of 10.6 cm located SW of the epicenter. The position of the epicenter is shown as a black circle. Figure 7b compares predicted ΔLOS using the preferred seismic slip model (figure 6b). The seismic slip model fails to model the magnitude of the ΔLOS displacement although it has adequate performance in terms of defining the region with greater than 20mm of ΔLOS displacement, as well as the orientation of the elliptical deformation. It is noted that the epicenter plots on the easternmost edge of the highest observed ΔLOS , which given the SE dip of the rupture plane would require the slip to be located updip of the hypocenter contrary to the seismic inversion results.

We determined a preliminary geodetic slip model using the ΔLOS data assuming an elastic half-space, and strike/dip of 40/55 degrees. The resultant slip distribution is shown in figure 8 and is similar to the seismic results (figure 6b) except the entire slip patch is shifted about 5 km shallower. The maximum slip is 81.9 cm, and the scalar seismic moment is 1.68×10^{25} dyne cm (M_w 6.1). Like the seismic models the slip is concentrated southeast of the hypocenter.

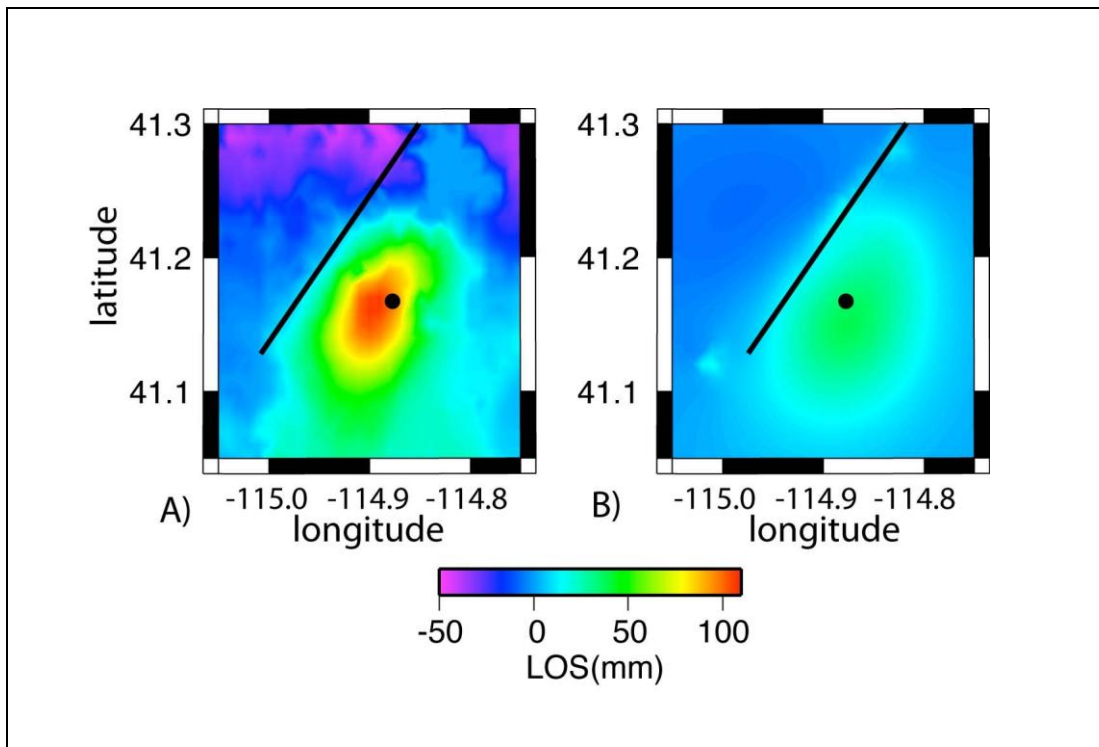


Figure 7. A) Line-of-sight (LOS) displacement from unwrapped ascending orbit ALOS interferograms for the period from December 19, 2007 to March 30, 2008. B) Estimated ΔLOS displacement for the preferred seismic slip model (figure 6b). The black lines are for reference comparing.

A possible explanation for the depth discrepancy between the geodetic and seismic slip models is that the hypocenter location, and therefore the assumed fault plane location are both in error. As noted previously, the epicenter lies to the east of the maximum ΔLOS while the seismic slip is located SE of the epicenter (slightly down dip from the hypocenter). We performed cursory sensitivity tests with respect to the position of the fault plane, and found that shifting the fault plane by approximately 2.5 km to the west caused the geodetic slip to locate at the same depth as in the seismic model.

There are also several other possible reasons for the discrepancy between the seismic and geodetic finite-source inversion, which include: adjustments to the timing of the seismic waveform data, the use of a half space vs. layered elastic structure, and the possibility that the SAR data includes a post-seismic signal. Since the post-event scene is March 20, 2008, approximately one month after the event, the observed SAR ΔLOS (figure 7a) could therefore be larger than predicted by the preferred seismic model (figure 7b) due to unaccounted-for, post-seismic deformation.

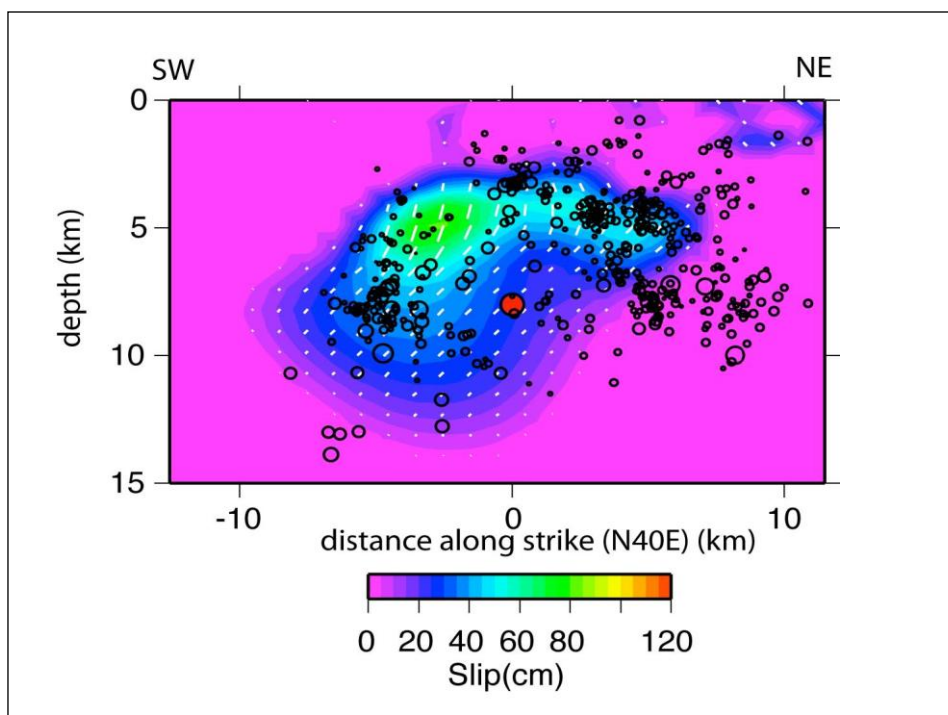


Figure 8. Slip obtained by inverting the Δ LOS displacements shown in figure 7 in a half-space elastic model. Relocated aftershocks (Smith and others, 2008) are plotted as black circles and the slip direction by a white line. The position of the hypocenter (red circle) is given for reference.

Future work will need to focus on reconciling the differences between the seismic and geodetic slip models, testing the sensitivity of the models to the various causes listed above, as well as performing a simultaneous inversion of both data sets.

WELLS STRONG MOTIONS

There were no direct observations of strong ground motion in the town of Wells, Nevada. Using the finite-source model shown in figure 6b, we simulated strong ground motion records over a grid of stations (figure 9a). Since the Song and others (1996) velocity model has hard rock velocities at the surface, we adjusted the amplitude of the motions to correspond to a NEHRP Class C site. We approximate the site amplification by considering the transmission coefficient from the 2.05 km/s (hard rock) layer in the Song and others (1996) velocity model (table 1) to the median shear wave velocity for a NEHRP Class C site (564 m/s). Considering the density of the rock (table 1) and assuming a density of 2 g/cc for the stiff soil we obtain a frequency independent amplification factor of 1.6, which was applied to the simulated hard rock synthetic ground motions.

The maximum peak horizontal ground velocity (PGV) of 13.5 cm/s occurs 10 km southwest of the epicenter near Wells. PGV exceeding 10 cm/s corresponds to the onset of damage to unreinforced masonry buildings. Such buildings in the historic district were heavily damaged. As shown by dePolo (2008), in addition to the significant damage of the historic district, there were examples of westward sliding and toppling of heavy objects and chimneys. Figure 9b shows three-component displacement waveforms simulated for Wells, which shows that the finite-source slip model predicts on the order of 0.5 cm of static deformation to the east, north, and down that occurs over a span of 2-3 seconds. The simulated direction of motion of the far-field waves and the intermediate-field static motions are consistent with the observed sliding and toppling directions.

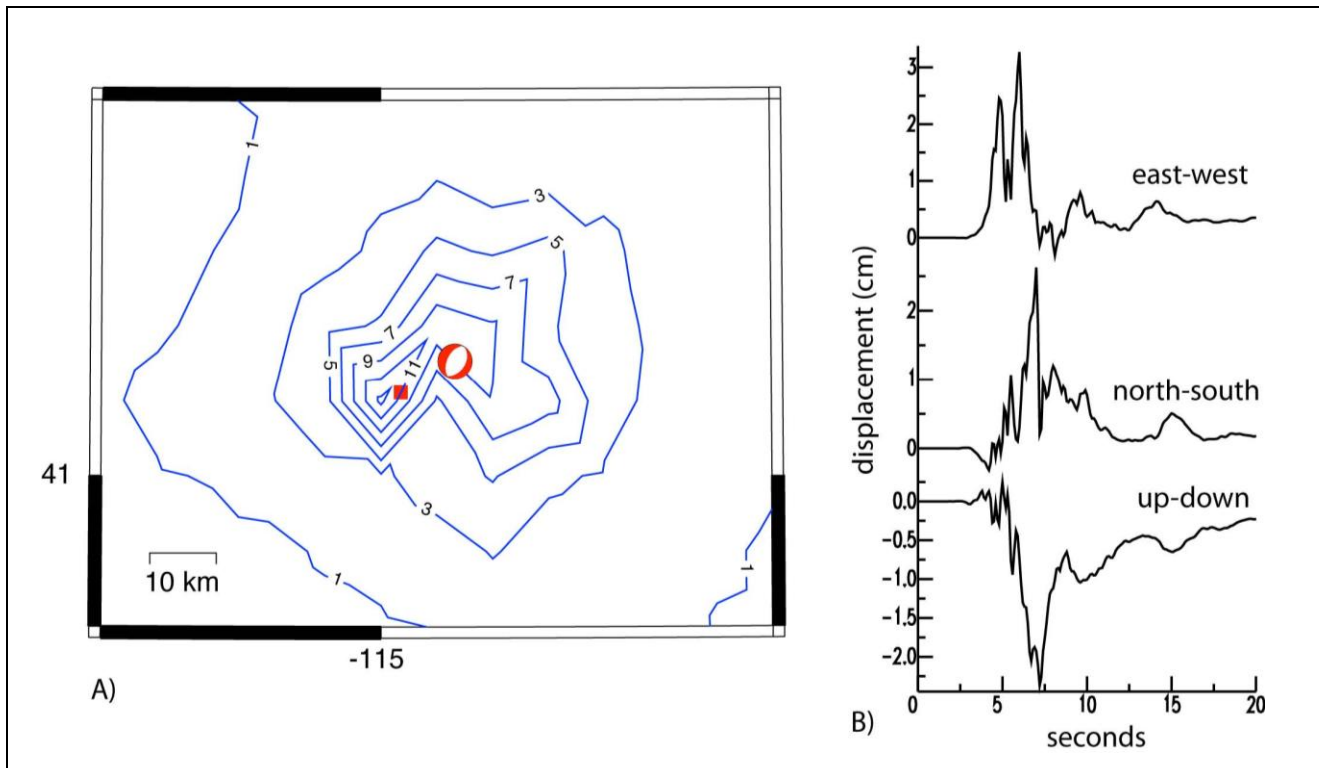


Figure 9. A) Simulated PGV (cm/s) scaled to a NEHRP Class C site. The elevated PGV lobes to the SW and SE are due to the SH radiation pattern and directivity. Wells Nevada is indicated by the red square. The focal mechanism marks the epicenter. B) Three-component displacement synthetics for Wells, Nevada (approximately 10 km SW of the epicenter). The solution predicts approximately 0.5 cm of static deformation to the east, north, and down.

CONCLUSION

A finite-source model was determined for the 21 February 2008 Wells, Nevada earthquake using three-component waveform data from the EarthScope Transportable Array. The preferred model uses a fault plane orientation inferred from the Smith and others (2008) relocation of aftershocks. The model shows that the primary slip patch is located approximately 3 km down dip, and 5 km SE of the hypocenter located at 7 km depth. Slip occurs over a narrow depth range (5-11 km), in a region with fewer aftershocks. While the rupture was bilateral the greatest slip is located SW of the hypocenter resulting in directivity amplification in Wells with estimated PGV in Wells exceeding 10 cm/s.

ACKNOWLEDGMENTS

This is BSL contribution 10-02. We thank Chen Ji, and an anonymous reviewer for helpful criticisms and suggestions.

REFERENCES

- dePolo, C., 2008, Observations and Reported Effects of the February 21, 2008 Wells, Nevada, Earthquake, 03/15/2008, UNR.
- Dreger, D., and Kaverina, A., 2000, Seismic remote sensing for the earthquake source process and near-source strong shaking—A case study of the October 16, 1999 Hector Mine earthquake: *Geophysical Research Letters*, v. 27, p. 1941–1944.
- Ford, S.R., Dreger, D.S., and Walter, W.R., 2009, Identifying isotropic events using a regional moment tensor inversion: *Journal of Geophysical Research*, v.114, p. 381-389, B01306, doi:10.1029/2008JB005743.
- Hartzell, S. H., and Heaton, T. H., 1983, Inversion of strong ground motion and teleseismic waveform data for the fault rupture history of the 1979 Imperial Valley, California, earthquake: *Bulletin of the Seismological Society of America*, v. 73, p. 1553–1583.

- Kaverina, A., Dreger, D. and Price, E., 2002, The combined inversion of seismic and geodetic data for the source process of the 16 October 1999 M_W 7.1 Hector Mine, California, Earthquake: *Bulletin of the Seismological Society of America*, v. 92, no. 4, p.1266-1280.
- Minson, S., and Dreger, D., 2007, Stable inversions for complete moment tensors: *Geophysical Journal International*, v.174, p.585–592, doi:10.1111/j.1365-246X.2008.03797.x.
- Okada, Y., 1985, Surface deformation due to shear and tensile faults in a half-space: *Bulletin of the Seismological Society of America*, v. 75, p.1135–1154.
- Song, X.J., Helmberger, D.V., and Zhao, L., 1996, Broad-band modeling of regional seismograms—the Basin and Range crustal structure, *Geophysical Journal International*, v.125, no.1, p. 15–29.
- Smith, K., dePolo, C., Torrisi, J., Edwards, N., Biasi, G., and Slater, D., 2008, The 2008 M_W 6.0 Wells, Nevada, Earthquake [abs]: 2008 Fall AGU Meeting, San Francisco, abstract #S51B-1741.